THE ASTROPHYSICAL JOURNAL, 552:731–737, 2001 May 10

OPTICAL GRAVITATIONAL LENSING EXPERIMENT: DIFFERENCE IMAGE ANALYSIS OF OGLE-2000-BUL-43, A SPECTACULAR ONGOING PARALLAX MICROLENSING EVENT[1]

I. SOSZYŃSKI,[2,3] K. ŻEBRUŃ,[2,3] P. R. WOŹNIAK,[3] S. MAO,[4] A. UDALSKI,[2] M. SZYMAŃSKI,[2] M. KUBIAK,[2]
G. PIETRZYŃSKI,[2,5] O. SZEWCZYK,[2] AND Ł. WYRZYKOWSKI[2]
Received 2000 December 7; accepted 2001 January 12

ABSTRACT

We present the photometry and theoretical models for a Galactic bulge microlensing event, OGLE-2000-BUL-43. The event is very bright, with $I = 13.54$ mag, and has a very long timescale, $t_E = 156$ days. The long timescale and its light curve deviation from the standard shape strongly suggest that it may be affected by the parallax effect. We show that OGLE-2000-BUL-43 is the first discovered microlensing event, in which the parallax distortion is observed over a period of 2 yr. Difference image analysis (DIA) using the PSF matching algorithm of Alard & Lupton enabled photometry accurate to 0.5%. All photometry obtained with DIA is available electronically. Our analysis indicates that the viewing condition from a location near Jupiter will be optimal and could lead to magnifications of ~ 50 around 2001 January 31. These features offer a great promise for resolving the source (a K giant) and breaking the degeneracy between the lens parameters, including the mass of the lens, if the event is observed with the imaging camera on the *Cassini* space probe.

Subject headings: gravitational microlensing — methods: data analysis

On-line material: color figures

1. INTRODUCTION

Gravitational microlensing was originally proposed as a method of detecting compact dark matter objects in the Galactic halo (Paczyński 1986). However, it also turned out to be an extremely useful method for studying Galactic structure, mass functions of stars, and potential extrasolar planetary systems (for a review, see Paczyński 1996). Most microlensing events are well described by the standard light curve (e.g., Paczyński 1986). Unfortunately, from these light curves, one can derive only a single physical constraint, namely, the Einstein radius crossing time, which involves the lens mass, various distance measures, and relative velocity (see § 4). This degeneracy means that the lens properties cannot be uniquely inferred. Therefore, any further information on the lens configuration is of great importance. Microlensing events that exhibit parallax effects provide this type of information. Such effects can occur when the event is observed simultaneously from two different positions in the solar system (Refsdal 1966), or when the event lasts long enough that the Earth's motion can no longer be approximated as rectilinear during the event (Gould 1992). Both of these effects will be directly relevant to the current paper. The first parallax microlensing event was reported by the MACHO collaboration toward the Galactic bulge (Alcock et al. 1995), and the second case (toward Carina) was discovered by the OGLE collaboration and reported in Mao (1999). Additional parallax microlensing candidates have been presented in a conference proceeding (Bennett et al. 1997). In this paper, we report a new parallax microlensing event, OGLE-2000-BUL-43. This bulge event was discovered well ahead of the peak by the Early Warning System (Udalski et al. 1994), and attracted attention because of its extreme brightness and very long timescale.

The unusually long duration of the event ($t_E \sim 156$ days), combined with the extremely small velocity of the magnification pattern on the plane of the observer ($\tilde{v} \sim 40$ km s^{-1}, i.e., hardly faster than the motion of the Earth), imply that the parallax effect is not only detectable, but is measurable very precisely. To make the most of this possibility, we employ difference image analysis (DIA; Woźniak 2000) to optimize the photometry (§ 2).

The parallax measurement that we present here yields not only the size of the Einstein radius projected onto the observer plane ($\tilde{r}_E \approx 3.62$ AU), but also the direction of lens-source relative motion in the heliocentric coordinate system. By combining these two, we can predict the light curve seen by any observer in the solar system as a function of time. In particular, we predict that as seen from the *Cassini* spacecraft around 2001 January 31, the lens and source will have an extraordinarily close separation, and hence the source will be highly magnified. Unless the lens turns out to be very massive ($M \gtrsim 0.8\, M_\odot$) and close ($D_l \lesssim$ 1 kpc), such a separation would permit resolution of the source and hence measurement of the angular Einstein radius, θ_E (Alcock et al. 1997, 2000; Albrow et al. 1999, 2000, 2001; Afonso et al. 2000). Gould (1992) showed that by combining measurements of $\tilde{r}_E$, θ_E, and the Einstein radius crossing time (t_E), one could obtain a complete solution of the event,

$$M = \frac{c^2}{4G}\,\tilde{r}_E\,\theta_E\,, \tag{1}$$

$$D_{\rm rel} = \frac{\tilde{r}_E}{\theta_E} \equiv \frac{\rm AU}{\pi_{\rm rel}}\,, \tag{2}$$

[1] Based on observations obtained with the 1.3 m Warsaw Telescope at the Las Campanas Observatory of the Carnegie Institution of Washington.

[2] Warsaw University Observatory, Al. Ujazdowskie 4, 00-478 Warszawa, Poland; soszynsk@astrouw.edu.pl, zebrun@astrouw.edu.pl, udalski@astrouw.edu.pl, msz@astrouw.edu.pl, mk@astrouw.edu.pl, pietrzyn@astrouw.edu.pl, szewczyk@astrouw.edu.pl, wyrzykow@astrouw.edu.pl.

[3] Princeton University Observatory, Princeton, NJ 08544-1001; soszynsk@astro.princeton.edu, zebrun@astro.princeton.edu, wozniak@astro.princeton.edu.

[4] University of Manchester, Jodrell Bank Observatory, Macclesfield, Cheshire SK11 9DL, UK; smao@jb.man.ac.uk.

[5] Universidad de Concepción, Departamento de Fisica, Casilla 160-C, Concepción, Chile.

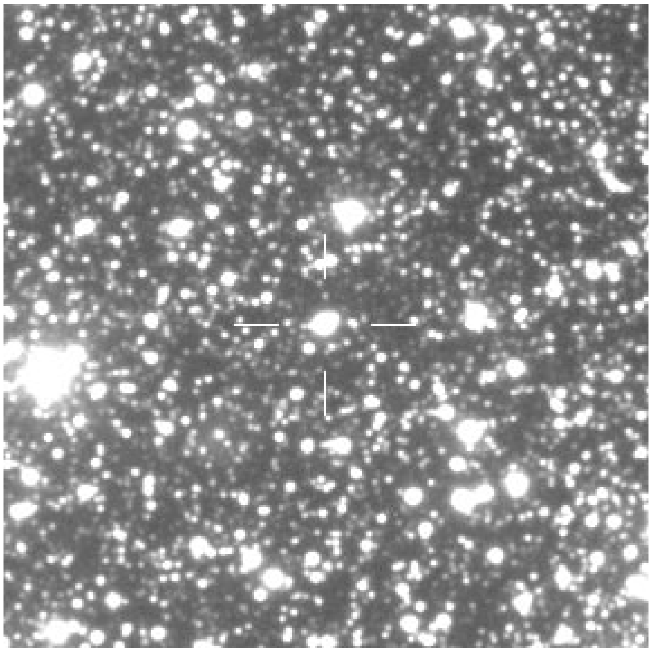

FIG. 1.—Finding chart for the OGLE-2000-BUL-43 microlensing event. The size of the I-band subframe is $120'' \times 120''$; north is up and east to the left.

$$\mu_{\rm rel} = \frac{\theta_{\rm E}}{t_{\rm E}} , \tag{3}$$

where $D_{\rm rel} = D_l D_s/(D_s - D_l)$, $\pi_{\rm rel} = {\rm AU}/D_l - {\rm AU}/D_s$ is the lens-source relative parallax, $\mu_{\rm rel}$ is the lens-source relative proper motion, and D_l and D_s are the distances to the lens and source, respectively. See also Gould (2000). Since the source is quite bright even at baseline ($I = 13.54$, $V = 15.65$), it should be easily measurable by the *Cassini* probe. *Cassini* photometry would therefore very likely yield the first mass measurement of a microlensing event.

The outline of the paper is as follows. In § 2 we describe observations; in § 3 we describe our photometric reduction method; § 4 contains the details of model fitting and predicted viewing conditions; in § 5 we describe potential scientific returns of *Cassini* observations; and finally, in § 6 we briefly summarize and discuss our results.

2. OBSERVATIONS

All observations presented in this paper were carried out during the second phase of the OGLE experiment with the 1.3 m Warsaw telescope at the Las Campanas Observatory, Chile, which is operated by the Carnegie Institution of Washington. The telescope was equipped with the "first-generation" camera with a SITe 2048×2048 CCD detector working in the drift-scan mode. The pixel size was 24 μm, giving the scale of $0\farcs417$ per pixel. Observations of the Galactic bulge fields were performed in the "medium" reading mode of the CCD detector with the gain 7.1 e^- per ADU and readout noise of about 6.3 e^-. Details of the instrumentation setup can be found in Udalski, Kubiak, & Szymański (1997).

The OGLE-2000-BUL-43 event was detected by the OGLE Early Warning System (Udalski et al. 1994) in mid-2000. Equatorial coordinates of the event for 2000.0 epoch are $\alpha_{2000} = 18^{\rm h}08^{\rm m}43\fs04$, $\delta_{2000} = -32°24'39\farcs5$; ecliptic coordinates are $\lambda = 271\fdg863$, $\beta = -8\fdg986$; and Galactic coordinates are $l = 359\fdg467$, $b = -6\fdg036$. Figure 1 is a finding chart showing the $120'' \times 120''$ region centered on the event. Observations of this field started in 1997 March and continued until 2000 November 22. The bulge observing season usually ends at the beginning of November; therefore, the latest observations of OGLE-2000-BUL-43 were made in difficult conditions, with the object setting shortly after the sunset, when the sky is still quite bright. Fortunately, the source was bright enough so that poor seeing and high backgrounds were not a significant problem in the DIA analysis.

The majority of the OGLE-II frames are taken in the I-band. For the BUL_SC7 field, 330 I-band and nine V-band observations were collected. Udalski et al. (2000) gives full details of the standard OGLE observing techniques, and the DoPHOT photometry is available from the OGLE Web site.[6]

3. PHOTOMETRY

Our analysis includes all I-band observations of the BUL_SC7 field. We used the DIA technique to obtain the light curves of the OGLE-2000-BUL-43 event. Our method is based on the recently developed optimal PSF matching algorithm (Alard & Lupton 1998; Alard 2000). Unlike other methods, which use divisions in Fourier space (Crotts 1992; Phillips & Davis 1995; Tomaney & Crotts 1996; Reiss et al. 1998; Alcock et al. 1999), the Alard & Lupton method operates directly in real space. In addition, it is not required to know the PSF of each image to determine the convolution kernel. Woźniak (2000) tested the method on large samples and showed that the error distribution is Gaussian to better than 1%. Compared to the standard DoPhot photometry (Schechter, Mateo, & Saha 1993), the scatter was always improved by a factor of 2–3, and frames taken in even the worst seeing conditions gave good photometric points.

Our DIA software handles PSF variations in drift-scan images by polynomial fits. Even then, it is necessary to subdivide the frames into 512×128 pixel strips, because PSF variability along the direction of the scan is much faster than across the frame. The object of interest turned out to be not too far from the center of one of the subframes selected automatically; therefore, we basically adopted the standard pipeline output for that piece of the sky, without needing to run the software on the full format. Minor modifications included more careful preparation of the reference image and calibration of the counts in terms of a standard magnitude system.

First, from the full data set for the BUL_SC7 field we selected 20 frames with the best seeing, small shifts relative to OGLE template, and low background level. More weight was assigned to the PSF shape and quality of telescope tracking in the analyzed region during the selection process. These frames were coadded to create a reference frame for all subsequent subtractions. Preparation of the reference image was absolutely critical for the quality of the final results.

Next, we ran the DIA pipeline for all of our data to retrieve the AC signal (variable part of the flux) of our lensed star. The software rejected only nine frames because

[6] OGLE web site is available at: http://www.astrouw.edu.pl/~ogle/ogle2/ews/ews.html.

of very bad observing conditions or very large shifts with respect to the reference image. Our final light curve contains 321 observations. To calibrate the result on the magnitude scale, we ran DoPhot on the reference image. The magnitude zero point ($I = 13.54$, $V = 15.65$) was obtained by comparing our DoPhot photometry with the OGLE database.

The DIA light curve is shown in Figure 2. The scatter in the photometry is 0.5% and is dominated by systematics due to atmospheric turbulence and PSF variations. The individual error bars returned by the automated massive photometry pipeline (Woźniak 2000) proved to be overestimated when compared to the scatter around the best-fit model (§ 4). Most likely, this is a combined result of individual care during data processing for OGLE-2000-BUL-43 and the relatively low density of stars in the BUL_SC7 field. The errors were recalibrated so as to force the χ^2 per degree of freedom to be unity in the best-fit model with parallax (see § 4 and Table 1).

We would like to stress the fact that it is the accuracy achieved here with the DIA method that enabled a detailed study of the lens parameters. Figure 3 presents the distribution of residuals with respect to the model (see § 4) for measurements with the DIA pipeline. Maximal differences between the classical single-point microlensing model and the parallax fit are indicated by dashed vertical lines. Note that the scatter of the photometry is small enough to analyze the parallax effect. In addition, our data set contains 82 more points than the OGLE EWS light curve. The difference is because the lowest grade frames are rejected in the standard DoPhot analysis. The DIA photometry data file is available from the OGLE anonymous FTP server.[7]

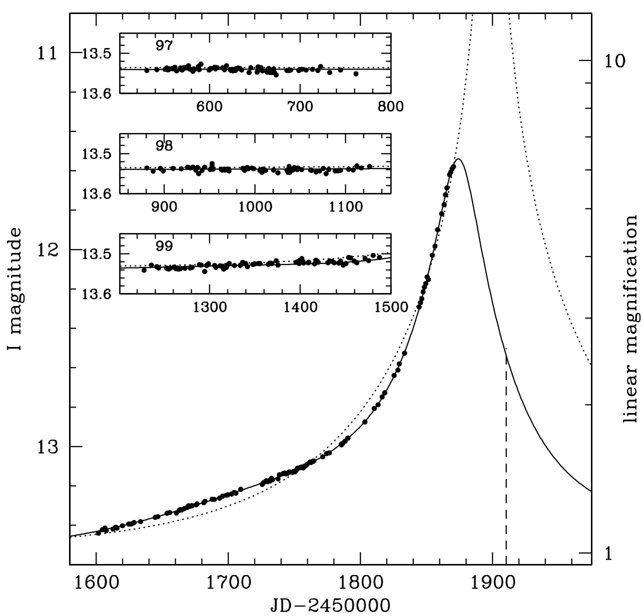

FIG. 2.—*I*-band light curve for the microlensing event OGLE-2000-BUL-43. The magnitude scale is shown on the left *y*-axis, while linear magnification is shown on the right *y*-axis. The dotted line shows the standard model, while the solid line shows the best-fit model that takes into account the parallax effect and blending (second row in Table 1). The vertical dashed line marks 2001 January 1, 0 UT. The three insets show the data points for the 1997, 1998, and 1999 seasons, respectively. [*See the electronic edition of the Journal for a color version of this figure.*]

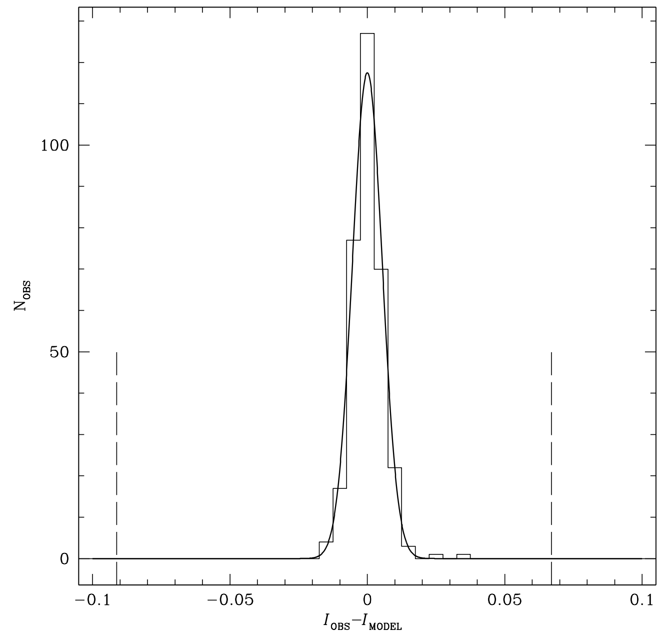

FIG. 3.—Distribution of residuals with respect to the model for measurements with the DIA pipeline. Width of the bin is 0.005 mag. The σ of fitted Gaussian is 0.0055 mag. Additional dashed vertical lines indicate the largest differences between the classical single-point microlensing model and the parallax fit.

In Figure 4 we present the color-magnitude diagram for the BUL_SC7 field. The position of the lensed star (marked by a cross) suggests that the source is a K giant. For later studies of the finite source size effect (§ 5), we would like to estimate the angular diameter of the star. In order to do this, we first need to estimate the dereddened color and magnitude of the star. For this purpose, we use the red-clump giants that have well-calibrated dereddened colors and magnitudes. We adopt the average color and magnitude of red-clump giants in Baade's window from the pre-

[7] The photometry data file is available at: ftp://sirius.astrouw.edu.pl/ogle/ogle2/BUL-43/bul43.dat.gz.

TABLE 1

STANDARD AND PARALLAX MODELS FOR OGLE-2000-BUL-43

Model	t_0	t_E (day)	u_0	I_s	ψ	$\tilde{r}_E$ (AU)	f	χ^2
S	1898.7 ± 0.1	169.6 ± 0.3	0.0 ± 0.002	13.5366 ± 0.0004	...	...	...	9025.2
P	1893.4 ± 1.0	156.4 ± 4.4	0.27 ± 0.01	13.5406 ± 0.0004	3.024 ± 0.005	3.62 ± 0.18	0.911 ± 0.056	314
P′......	1842.5 ± 0.9	158.2 ± 4.2	−0.11 ± 0.01	13.5406 ± 0.0004	3.017 ± 0.007	4.79 ± 0.22	0.77 ± 0.04	320.8

NOTE.—S: Best standard model; P: best parallax model with blending; P′: parallax fit with slightly worse χ^2 (see § 6).

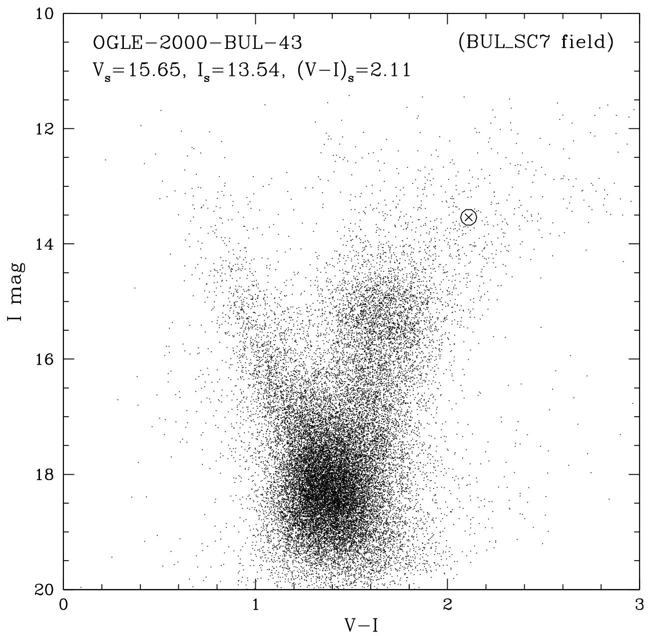

FIG. 4.—Color-magnitude diagram of the BUL_SC7 field. Only about 10% of field stars are plotted by tiny dots. Position of OGLE-2000-BUL-43 event is marked by the circled cross.

vious studies (Paczyński et al. 1999),

$$(V-I)_{\rm RC,0} = 1.11, \quad I_{\rm RC,0} = 14.37 . \qquad (4)$$

From Figure 4, the red-clump stars in the BUL_SC7 field have

$$(V-I)_{\rm RC} = 1.67 \pm 0.02, \quad I_{\rm RC} = 15.15 \pm 0.05 . \qquad (5)$$

Hence, we have

$$E(V-I) = (V-I)_{\rm RC} - (V-I)_{\rm RC,0} = 0.57 , \qquad (6)$$

and

$$A_I = I_{\rm RC} - I_{\rm RC,0} = 0.78 . \qquad (7)$$

Taking into account a blending parameter $f = 0.91$ (see § 4, Table 1) in the I band, we obtain the magnitudes of the lensed star as $I = 13.64$, $V = 15.75$. Hence, the intrinsic color and I-band magnitude for OGLE-2000-BUL-43 are

$$(V-I)_0 = (V-I) - E(V-I) = 1.54 ,$$
$$I_0 = I - A_I = 12.86 . \qquad (8)$$

Note that these values we derived are somewhat different from those of Schlegel, Finkbeiner, & Davis (1998), $A_I = 0.92$ and $E_{V-I} = 0.61$. Our smaller extinction value is consistent with Stanek (1998), who argued that the Schlegel et al. (1998) map overestimates the extinction for $|b| < 5°$. Our estimate based on the red-clump giants is also somewhat uncertain because of the metallicity gradient that may exist between Baade's window ($b = -4°$) and the BUL_SC7 field ($b = -6°$). Fortunately, this uncertainty in reddening only affects the angular diameter estimate very slightly because the surface brightness-color relation has a slope similar to the slope of the reddening line (see below).

Using the dereddened color and magnitude, we can estimate the angular stellar radius (θ_*) using the empirically determined relation between color and surface brightness (van Belle 1999), independent of the source distance. Transforming van Belle's relation given in V versus $V-K$ into I versus $V-I$ using the color-color relations of Bessel & Brett (1988), one obtains

$$\theta_* = 18.9\ \mu{\rm as} \times 10^{(12.90 - I_0)/5}[(V-I)_0 - 0.6] . \qquad (9)$$

For our star, this gives $\theta_* = 18.1$ μas. Using the values from Schlegel et al. (1998), the θ_* value increases by about 2%. Therefore, the estimate of the angular stellar radius is quite robust.

4. MODEL

We first fit the light curve with the standard single microlens model, which is sufficient to describe most microlensing events. In this model, the (point) source, the lens, and the observer all move with constant spatial velocities. The standard form is given by (e.g., Paczyński 1986)

$$A(t) = \frac{u^2 + 2}{u\sqrt{u^2 + 4}} , \quad u(t) \equiv \sqrt{u_0^2 + \tau(t)^2} , \qquad (10)$$

where u_0 is the impact parameter (in units of the Einstein radius) and

$$\tau(t) = \frac{t - t_0}{t_{\rm E}} , \quad t_{\rm E} = \frac{\theta_{\rm E}}{\mu_{\rm rel}} , \qquad (11)$$

where t_0 is the time of the closest approach (maximum magnification), $\theta_{\rm E}$ is the angular Einstein radius, and $t_{\rm E}$ is the Einstein radius crossing time. The explicit forms of the angular Einstein radius ($\theta_{\rm E}$) and the projected Einstein radius ($\tilde{r}_{\rm E}$) are

$$\theta_{\rm E} = \sqrt{\frac{4GM}{c^2 D_{\rm rel}}} , \quad \tilde{r}_{\rm E} = \sqrt{\frac{4GMD_{\rm rel}}{c^2}} , \qquad (12)$$

where M is again the lens mass and $D_{\rm rel}$ is defined below equation (3). For microlensing in the local group, $\theta_{\rm E}$ is $\sim$mas and $\tilde{r}_{\rm E}$ $\sim$a few AU. Equations (10)–(12) show the well-known lens degeneracy, i.e., from a measured $t_{\rm E}$, one cannot infer the lens mass, distances, and kinematics uniquely even if the source distance is known.

To fit the I-band data with the standard model, we need a minimum of four parameters, namely, u_0, t_0, $t_{\rm E}$, and I_s, where I_s is the unlensed I-band magnitude of the source. The best-fit parameters (and their errors) are found by minimizing the usual χ^2 using the MINUIT program in the CERN library[8] and are tabulated in Table 1 (model S). The resulting χ^2 is 9025.2 for 317 degrees of freedom. The large χ^2 indicates that the fit is unacceptable. This can also be clearly seen in Figure 2, where we have plotted the predicted light curve by a dotted line. The deviation is apparent in the 2000 observing season. In fact, upon closer examination, the model overpredicts the magnification in the 1999 season as well (see the bottom inset in Fig. 2). Since the Galactic bulge fields are very crowded, there could be some blended light from a nearby unlensed source within the seeing disk of the lensed source, or there could be some light from the lens itself. Thus, in the model we can introduce a blending parameter, f, which we define as the fraction of light contributed by the lensed source in the baseline ($f = 1$ if there is no blending). Note that blending is introduced in our adoption of the magnitude zero point obtained by the DoPhot pho-

[8] CERN library is available at: http://wwwinfo.cern.ch/asd/cernlib/.

tometry; the DIA method itself automatically subtracts out the blended light. The inclusion of the blending parameter reduces the χ^2 to 2778.4 for 316 degrees of freedom. This model requires a blending fraction $f = 0.22$, which is implausible considering the extreme brightness of the lensed star. In any case, the χ^2 is better but still far from acceptable. We show below that all these discrepancies can be removed by incorporating the parallax effect.

To account for the parallax effect, we need to describe the Earth's motion around the Sun. We adopt a heliocentric coordinate system with the z-axis toward the ecliptic north and the x-axis from the Sun toward the Earth at the vernal equinox.[9] The position of the Earth, to first order of the orbital eccentricity ($\epsilon \approx 0.017$), is then (e.g., Dominik 1998, and references therein)

$$\begin{aligned} x_\oplus(t) &= A(t) \cos [\xi(t) - \phi_\gamma] , \\ y_\oplus(t) &= A(t) \sin [\xi(t) - \phi_\gamma] , \\ z_\oplus(t) &= 0 , \end{aligned} \tag{13}$$

where

$$A(t) = \mathrm{AU}(1 - \epsilon \cos \Phi), \quad \xi(t) = \Phi + 2\epsilon \sin \Phi \tag{14}$$

where $\Phi = 2\pi(t - t_p)/T$, $T = 1$ yr, and $\phi_\gamma \approx 75\overset{\circ}{.}98$ is the longitude difference between the perihelion ($t_p = 1546.708$) and the vernal equinox ($t \equiv \mathrm{JD} - 2450000 = 1623.816$) for J2000. The line of sight in the heliocentric coordinate system is as usual described by two angular polar coordinates (ϕ, χ). These two angles are related to the geocentric ecliptic coordinates (λ, β) by $\chi = \beta$ and $\phi = \pi + \lambda$. Again, for OGLE-2000-BUL-43, $\beta = -8\overset{\circ}{.}986$ and $\lambda = 271\overset{\circ}{.}863$ (see, e.g., Lang 1981 for conversions between different coordinate systems).

To describe the lens parallax effect, we find it more intuitive to use the natural formalism as advocated by Gould (2000), i.e., we project the usual lensing quantities into the observer (and ecliptic) plane. The line-of-sight vector is given by $\hat{\boldsymbol{n}} = (\cos \chi \cos \phi, \cos \chi \sin \phi, \sin \chi)$ in the heliocentric coordinate system. For a vector $\boldsymbol{r}$, the component perpendicular to the line of sight is given by $\boldsymbol{r}_\perp = \boldsymbol{r} - (\boldsymbol{r} \cdot \hat{\boldsymbol{n}})\hat{\boldsymbol{n}}$. For example, the perpendicular component of the Earth position is $\boldsymbol{r}_{\oplus,\perp} = \boldsymbol{r}_\oplus - (\boldsymbol{r}_\oplus \cdot \hat{\boldsymbol{n}})\hat{\boldsymbol{n}}$. Thus, a circle in the lens plane ($r_\perp^2 = R^2$) is mapped into an ellipse in the ecliptic plane, which is given by

$$r = \frac{R}{\sqrt{1 - \cos^2 \chi \cos^2 (\Theta - \phi)}} , \tag{15}$$

where Θ is the polar angle in the ecliptic plane. The minor and major axes for the ellipse are R and $R/\sin \chi$, respectively.

The lens trajectory is described by two parameters, the dimensionless impact parameter, u_0, and the angle, ψ, between the heliocentric ecliptic x-axis and the normal to the trajectory. Note that u_0 is now more appropriately the (dimensionless) minimum distance between the Sun-source line and the lens trajectory. For convenience, we define the Sun to be on the left-hand side of the lens trajectory for $u_0 > 0$. The lens position (in physical units) projected into the ecliptic plane, $\boldsymbol{r}_l = (x_l, y_l, 0)$, as a function of time, is given by

$$\begin{aligned} x_l &= u_0 \tilde{r}_\mathrm{E} \cos \psi - \tau r_{\mathrm{E},p}(\psi) \sin \psi , \\ y_l &= u_0 \tilde{r}_\mathrm{E} \sin \psi + \tau r_{\mathrm{E},p}(\psi) \cos \psi , \\ z_l &= 0 , \end{aligned} \tag{16}$$

where τ and $\tilde{r}_\mathrm{E}$ are defined in equations (11) and (12), and $r_{\mathrm{E},p} = \tilde{r}_\mathrm{E}/[1 - \cos^2 \chi \cos^2 (\pi/2 + \psi - \phi)]^{1/2}$ is the Einstein radius projected into the ecliptic plane in the direction of the lens trajectory. The expression of $r_{\mathrm{E},p}$ can be derived using equation (15) with $\Theta = \pi/2 + \psi$, where the factor $\pi/2$ arises because ψ is defined as the angle between the normal to the trajectory and the x-axis. We denote the vector from the lens position (projected into the ecliptic plane) toward the Earth as $\delta\boldsymbol{r} = \boldsymbol{r}_\oplus - \boldsymbol{r}_l$. The component of $\delta\boldsymbol{r}$ perpendicular to the line of sight is $\delta\boldsymbol{r}_\perp = \delta\boldsymbol{r} - (\delta\boldsymbol{r} \cdot \hat{\boldsymbol{n}})\hat{\boldsymbol{n}}$. The magnification can then be calculated using equation (10) with $u^2 = (\delta r_\perp/\tilde{r}_\mathrm{E})^2$.

In total, seven parameters (u_0, t_0, t_E, I_s, $\tilde{r}_\mathrm{E}$, ψ, f) are needed to describe the parallax effect with blending. These parameters are again found by minimizing χ^2. In Table 1, we list the best-fit parameters (model P); for this model, the χ^2 per degree of freedom is now unity as a result of our rescaling of errors (see § 3). In particular, we find that

$$\tilde{r}_\mathrm{E} = 3.62 \pm 0.16 \text{ AU}, \quad \psi = 3.024 \pm 0.005 \text{ rad} . \tag{17}$$

The correlation coefficient between $\tilde{r}_\mathrm{E}$ and ψ is -0.088. The predicted light curve is shown in Figure 2 as the solid line. The model fits the data points very well. Note that the model requires a marginal blending with $f = 0.911 \pm 0.056$. This is expected, since the source star is very bright, and it appears unlikely that any additional source can contribute substantially to the total light. We return to the degeneracy of solutions briefly in § 6.

Using equations (1) and (2), and $\tilde{r}_\mathrm{E} \approx 3.62$ AU, we obtain the lens mass as a function of the relative lens-source parallax,

$$M = \frac{c^2 \tilde{r}_\mathrm{E}^2}{4G} \pi_\mathrm{rel} = 0.23\ M_\odot\ 2\left(\frac{3.5 \text{ kpc}}{D_l} - \frac{7 \text{ kpc}}{D_s}\right) . \tag{18}$$

Thus, the lens is likely to be low-mass unless it is unusually close to us ($D_l \sim 1$ kpc). Combining $\tilde{r}_\mathrm{E}$ and t_E, we can also derive the projected velocity of the lens,

$$\tilde{v} = \mu_\mathrm{rel} D_\mathrm{rel} = \frac{\tilde{r}_\mathrm{E}}{t_\mathrm{E}} = 40 \pm 2 \text{ km s}^{-1} . \tag{19}$$

The low projected velocity favors a disk-disk lensing event. For such events, the observer, the lens, and the source rotate about the Galactic center with roughly the same velocity, and the relative motion is only due to the small, ~ 10 km s^{-1}, random velocities (see, e.g., Derue et al. 1999). On the other hand, the chance for a bulge source (with its much larger random velocity, ~ 100 km s^{-1}) to have such a low projected velocity relative to the lens (whether disk or bulge) is small. The low projected speed and the long duration of this event imply that the Earth's motion induces a large excursion in the Einstein ring, and this large deviation from rectilinear motion makes an accurate parallax measurement possible, even though the event has only barely reached its peak.

The accurate measurement of $\tilde{r}_\mathrm{E}$ and ψ makes it possible to predict the light curve that would be seen by a hypothetical observer anywhere in the solar system. Figure 5 shows

[9] Another commonly used heliocentric system (e.g., in the Astronomical Almanac 2000) has the x-axis opposite to our definition.

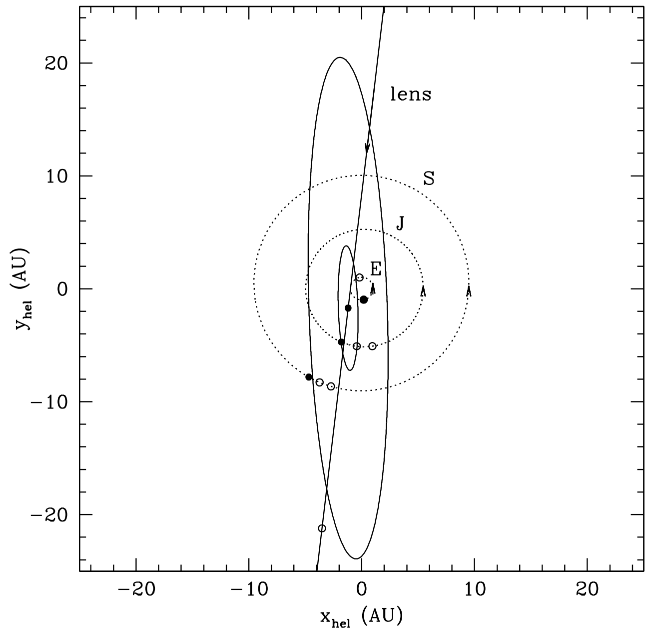

FIG. 5.—Illumination patterns for OGLE-2000-BUL-43 in the heliocentric ecliptic coordinates on 2001 January 1, 0 UT. The $+x$-axis points from the Sun toward the Earth on the day of vernal equinox. The two solid elliptical curves are the isomagnification contours with magnification 1.342 and 4, respectively. The three dotted circles show the orbits of the Earth, Jupiter, and Saturn, respectively. The solid filled circles on the Earth, Jupiter, and Saturn orbits indicate their positions on 2001 January 1, while the open circles indicate their positions every half-year in the future. The straight line indicates the lens trajectory, and the circles have the same meaning as those on the planetary orbits. The directions of motions are indicated by arrows. Note that the whole illumination pattern (isomagnification contours) comoves with the lens. [*See the electronic edition of the Journal for a color version of this figure.*]

the illumination pattern on 2001 January 1.000 UT. The two elliptical curves are isomagnification contours for $A = 1.342$ and 4, respectively; the outer contour with $A = 1.342$ corresponds to the Einstein "ring" in the ecliptic plane. It appears as an ellipse in Figures 5 and 7 because the ecliptic plane is not perpendicular to the source direction (cf. eq. [15]). Various filled circles indicate the positions of the source, Earth, Jupiter, and Saturn on this date. The open circles indicate the positions of the source and the planets every half-year in the future. From this figure, one can see that the inner contour nearly coincides with the position of Jupiter on 2001 January; hence, an observer close to Jupiter will see a magnification of about 4, and the magnification is even higher somewhat later. The *Cassini* probe is currently approaching Jupiter, for a fly-by acceleration on its way to Saturn; it is therefore an ideal instrument to observe this event from space. In the next section, we discuss in some detail the potential scientific returns of *Cassini* observations.

5. POTENTIAL SCIENTIFIC RETURNS OF *CASSINI* OBSERVATIONS

In Figure 6 we show the light curve of OGLE-2000-BUL-43 for an observer near Jupiter, mimicking the fly-by observations from *Cassini*. The light curve shows a spectacular peak at JD ≈ 2451940.5 (2001 January 31). Figure 7 illustrates the position of Jupiter with respect to the illumination pattern. It clearly shows that the lens and Jupiter will come very close together, and hence one will see a very high magnification around that time.

When the physical impact parameter is comparable to the stellar radius, microlensing light curves are substantially modified by the finite source size effect (Gould 1994; Nemiroff & Wickramasinghe 1994; Witt & Mao 1994). More

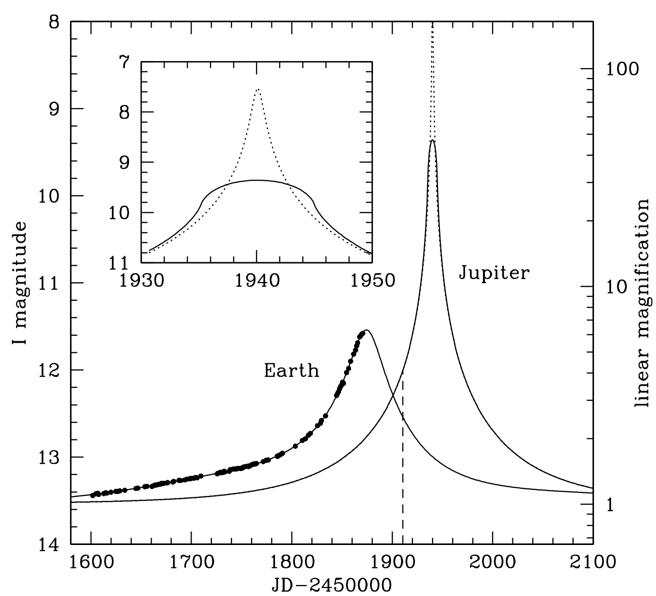

FIG. 6.—Light curve for OGLE-2000-BUL-43 as seen by an observer close to Jupiter. Note that it reaches a much higher peak around 2001 January 31 than that on the Earth. The vertical dashed line marks 2001 January 1, 0 UT (corresponding to the filled dots in Fig. 5). The magnitude scale is shown on the left y-axis, while linear magnification is shown on the right y-axis. The dotted line shows the magnification for a point source, while the solid line illustrates the finite source size effect. The inset shows the light curve close to the peak of the light curve. [*See the electronic edition of the Journal for a color version of this figure.*]

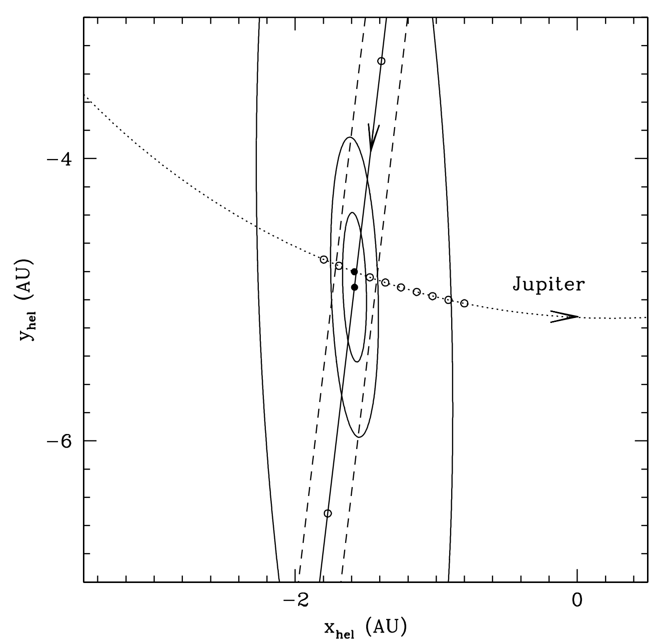

FIG. 7.—Illumination patterns for OGLE-2000-BUL-43 in the heliocentric ecliptic coordinates on 2001 January 31, 0 UT. Notations are similar to those in Fig. 5. The filled circles correspond to $t = 1840.5$, while the open circles are separated by 15 days. The contours correspond to magnifications of 5, 20, and 40 (from outer to inner). The two dashed lines bracket roughly the region that the finite source size effect can be observed. [*See the electronic edition of the Journal for a color version of this figure.*]

precisely, when

$$u_0 \lesssim u_* \equiv \frac{\theta_*}{\theta_E} = \frac{c^2}{4GM}\,\tilde{r}_E\,\theta_* = \frac{0.008}{M/M_\odot}\,, \qquad (20)$$

then finite source size effects will be significant and it becomes feasible to measure θ_E, hence providing one more constraint on the lens parameters. Our best-fit model has a minimum impact parameter (in the lens plane) of $u_0 = 3.6 \times 10^{-3}$, and so unless the lens is very close to us and very massive (eq. [18]), the finite source size will be resolved. The inset in Figure 6 illustrates this effect, where we have adopted $\theta_E = 0.47$ mas. The effect is quite dramatic. In comparison, the effect is negligible for an observer on Earth. Note that the peak of the light curve only depends on $u_* = \theta_*/\theta_E$. Thus, the peak can be higher if the angular Einstein radius is larger, and vice versa.

To plan space observations, it is important to estimate the errors in the minimum impact parameter (u_0) and the peak time (t_0). We have performed Monte Carlo simulations to estimate their uncertainties (e.g., Press et al. 1992). We find that the 95% confidence limits on u_0 and t_0 are $10^{-4} < u_0 < 0.011$ and $1938.3 < t_0 < 1941.3$, respectively. It is therefore very likely that the magnification at Jupiter will be very high. The peak time is accurate to about 3 days, while the finite source size effect lasts for about 20 days (see the inset in Fig. 6). To detect this effect, it is crucial to have at least a few observations during the lens transit across the stellar surface (Peng 1997). If the finite source size effect is indeed observed by *Cassini*, then we can measure θ_E, and this will lead, for the first time, to a complete solution of the lens parameters, including the lens mass, the relative lens-source parallax, and proper motions (see introduction). We again emphasize that the determination of mass is independent of the source distance if θ_E is measured (cf. eq. [1]).

6. SUMMARY AND DISCUSSION

OGLE-2000-BUL-43 is the longest microlensing event observed by the OGLE project. It is also the first event, in which the parallax effect is observed over a 2 yr period, making the association of the acceleration term with the motion of the Earth unambiguous. Photometric accuracy at the 0.5% level enabled a detailed study of the event parameters, partly removing the degeneracy between the mass, velocity, and distance. We conclude that the lens is slow moving, and unless it is unusually close to us, the lens mass is expected to be small.

The main aim of this paper is to strongly encourage further efforts to observe OGLE-2000-BUL-43, since this may lead the first complete determination of the lens parameters. We could even consider a confirmation of the predictions from Figure 6 to be an ultimate proof of our understanding of the microlensing geometry. This is particularly important since the lens model may not be unique. For example, we found another model (see Table 1, model P′) that has $\chi^2 = 320.8$ but with the blending parameter $f = 0.77$. This model predicts a much lower peak ($I_{\rm peak} = 12.2$) for an observer close to Jupiter. Even late space observations will be useful for distinguishing these two models. For example, the best-fit model predicts $I = 12.7$ and 13.0 on 2001 April 1 and May 1, respectively, while the slightly worse model predicts $I = 13.0$ and 13.2 on these dates. The difference between these two models can reach 0.02 mag in the next season for ground-based observations, and hence may be detectable from the ground as well. However, the alternative model appears physically unlikely, since the source star is so bright that one would expect f close to 1, as found in our best-fit model. The blending parameter may also be constrained by spectroscopic observations (Mao, Reetz, & Lennon 1998). A high-resolution VLT spectrum has already been taken and is currently being analyzed (K. Gorski 2000, private communication). It will shed further light on the stellar parameters (such as surface gravity) and the radial velocity of the lensed source.

We acknowledge Bohdan Paczyński for many inspiring discussions and comments on the manuscript. We are indebted to Andrew Gould for a prompt, detailed, and insightful referee's report that substantially improved the paper, particularly concerning the angular stellar radius estimate. We also thank Andrew Drake for many useful comments. This work was supported by the grants Polish KBN 2P03D00814 and NSF AST 98-20314.

REFERENCES

Afonso, C., et al. 2000, ApJ, 532, 340
Alard, C. 2000, A&AS, 144, 363
Alard, C., & Lupton, R. H. 1998, ApJ, 503, 325
Albrow, M. D., et al. 1999, ApJ, 522, 1022
———. 2000, ApJ, 534, 894
———. 2001, ApJ, 549, 749
Alcock, C., et al. 1995, ApJ, 454, L125
———. 1997, ApJ, 491, 436
———. 1999, ApJ, 521, 602
———. 2000, ApJ, 541, 270
Bennett, D. P., et al. 1997, BAAS, 191, 8303
Bessel, M. S., & Brett, J. M. 1988, PASP, 100, 1134
Crotts, A. 1992, ApJ, 399, L43
Derue, F., et al. 1999, A&A, 351, 87
Dominik, M. 1998, A&A, 329, 361
Gould, A. 1992, ApJ, 392, 442
———. 1994, ApJ, 421, L71
———. 2000, ApJ, 542, 785
Lang, K. R. 1981, Astrophysical Formulae (Berlin: Springer), 504
Mao, S. 1999, A&A, 350, L19
Mao, S., Reetz, J., & Lennon, D. J. 1998, A&A, 338, 56
Nemiroff, R. J., & Wickramasinghe, W. A. D. T. 1994, ApJ, 424, L21
Paczyński, B. 1986, ApJ, 304, 1
———. 1996, ARA&A, 34, 419
Paczyński, B., et al. 1999, Acta Astron., 49, 319
Peng, E. W. 1997, ApJ, 475, 43
Phillips, A. C., & Davis, L. E. 1995, ASP Conf. Ser. 77, Astronomical Data Analysis Software and Systems IV, ed. R. A. Shaw et al. (San Francisco: ASP), 297
Press, W. H., Teukolsky, S. A., Vetterling, W. T., & Flannery, B. P. 1992, Numerical Recipes in Fortran (New York: Cambridge Univ. Press), Chap. 15
Refsdal, S. 1966, MNRAS, 134, 315
Reiss, D. J., Germany, L. M., Schmidt, B. P., & Stubbs, C. W. 1998, AJ, 115, 26
Schechter, P. L., Mateo, M., & Saha, A. 1993, PASP, 105, 1342
Schlegel, D. J., Finkbeiner, D. P., & Davis, M. 1998, ApJ, 500, 525
Stanek, K. Z. 1998, preprint (astro-ph/9802307)
Tomaney, A. B., & Crotts, A. P. 1996, AJ, 112, 2872
Udalski, A., Kubiak, M., & Szymański, M. 1997, Acta Astron., 47, 319
Udalski, A., Szymański, M., Kałużny, J., Kubiak, M., Mateo, M., Krzemiński, W., & Paczyński, B. 1994, Acta Astron., 44, 227
Udalski, A., Żebruń, K., Szymański, M., Kubiak, M., Pietrzyński, G., Soszyński, I., & Woźniak, P. 2000, Acta Astron., 50, 1
van Belle, G. T. 1999, PASP, 111, 1515
Witt, H. J., & Mao, S. 1994, ApJ, 430, 505
Woźniak P. 2000, Acta Astron., submitted (preprint astro-ph/0012143)